Electromagnetic Propulsion System with Rapid Current Discharge Circuit for Enhanced Projectile Acceleration

Guy Bar Sovik, *Student Member*, Bar Halivni, *Student Member*, *IEEE*,
Michael Evzelman, *Member*, *IEEE,* and Mor Mordechai Peretz, *Member, IEEE*
The Center for Power Electronics and Mixed-Signal IC, Department of Electrical and Computer Engineering
Ben-Gurion University of the Negev, P.O. Box 653, Beer-Sheva, 8410501 Israel
sovik@post.bgu.ac.il barhal@post.bgu.ac.il evzelman@bgu.ac.il morp@ee.bgu.ac.il
http://www.ee.bgu.ac.il/~pemic

2022 IEEE 23rd Workshop on Control and Modeling for Power Electronics (COMPEL) | 978-1-6654-1081-6/22/$31.00 ©2022 IEEE | DOI: 10.1109/COMPEL53829.2022.9829983

***Abstract*— This paper presents a rapid current discharge circuit for single and multi-stage high current coilgun. The circuit eliminates an undesired braking force, which is developed due to a residual current, when the projectile passes the center point of an energized coil. This is done by rerouting the coil current towards an alternative, quick discharge path, where it is damped to zero. Utilization of the discharge circuit is especially advantageous in multi-stage coilgun systems, as the design of the discharge circuit is done once for the "worst case scenario" and applied to all the coils. It guarantees a safe operation of all the switches, with minor effect on the system performance. The discharge circuit operation has been validated by an experimental prototype rated for 450V, demonstrating rapid coil current discharge for braking force mitigation.**

Keywords – coilgun, current discharge circuit, muzzle velocity, braking force.

I. INTRODUCTION

Electromagnetic propulsion systems are extensively investigated in the last decades [1]-[11], due to their ability to accelerate payloads by converting electrical energy to kinetic energy, while avoiding combustive or chemical processes. The systems are commonly divided into two categories: railguns [12]-[14] and coilguns [15]-[18]. Railguns are built from two parallel conductors, and a sliding conducting armature. The current flows through the conductors and through the armature, and the resulting magnetic force pushes the armature. Coilguns are constructed by a coil wound around a barrel. The coil is driven by a pulsed power supply, and the magnetic field generated by the current carrying coil attracts a projectile towards its center.

In contrast to railgun technology, coilgun has almost no friction between the barrel and projectile, which reduces the possibility for rail erosion. However, a major setback of coilgun technology is the attraction of the projectile to the coil's center, which acts as a braking force after the projectile crosses the coil's middle point [19]. In certain cases, the projectile will reverse its direction, and might settle in the coil's center.

Overcoming the braking force applied on the projectile is possible with proper design. For a specific coil with known length and inductance, it is possible to adjust the capacitor's value and/or voltage, so that the current will reach zero before the projectile reaches the coil's center. Nevertheless, Due to the significant currents that are required to accelerate a projectile, it is extremely challenging to turn-OFF the switching-device at the vicinity of zero. Inaccurate timing may charge the parasitic capacitance of the switching-element instantly and damage it. Under these circumstances, it is greatly beneficial to use a switching-device that has a natural commutation characteristic [3]-[4].

Fig. 1 illustrates a single stage coilgun system, composed of a capacitor bank, *C*, a coil, *L*, and a SCR. *R* is the lumped loop resistance. To provide high current pulses the capacitor bank should have high-energy high-power characteristics, and as there are no commercially available products that serve these two purposes a hybrid capacitor approach which has been published in [3], has been adopted in this study. The hybrid capacitor is comprised of an electrolytic capacitor as the main energy source, and MLCCs for enhanced high-power characteristics. To avoid negative voltage, which can damage the polarized, electrolytic capacitor, a protection diode, D_{prot}, is added in parallel to the capacitor bank.

The high-energy high-power pulses generated by capacitor bank are expressed in very high currents in the coil, typically in the range of hundres-to-thousands Ampere, which may lead to distortion of the coil structure. A practical approach is to divide the coil into smaller segments, and drive each segment with a dedicated pulsed power supply [3], [8], [16], [19]-[20]. Such systems are referred to as multi-stage coilguns. Although a segmented approach eases the requirements of the drive stage, it introduces new complexities to the design and testing of such a system.

A multi-stage coilgun is depicted in Fig. 2. Every coil is driven by a dedicated drive stage, and a drive logic block determines the delay between pulses and the duration of each pulse. Normally, in practical systems, the drive stages are identical for all segments. However, the coil's length and

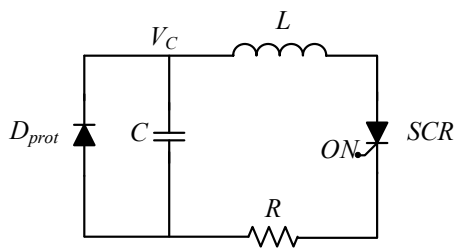

Fig. 1. Simplified block diagram of multi-stage coilgun.

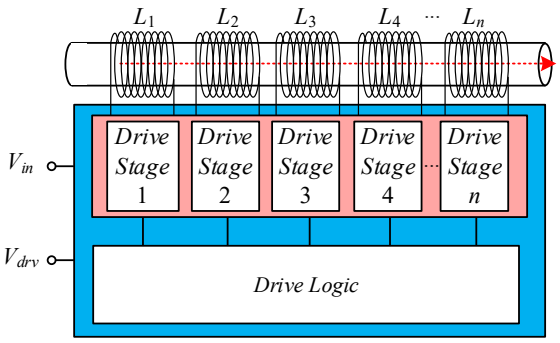

Fig. 2. Simplified block diagram of multi-stage coilgun.

inductance vary from stage to stage, and, as a result, it is possible to perfectly adjust only one segment of the multi-staged system, so that the current will reach zero before the projectile crosses its center. In the rest of the segments, deceleration of the projectile, due to a braking force, impairs the system's performance. An active current discharge circuit, which draws the coil current to zero, can mitigate the braking force effect in all the coil stages, and enhance the system's performance.

An active current discharge circuit may be achieved by redirecting the current to an alternative path, where it is damped to zero. Utilization of a discharge circuit is advantageous both to system performance, and to the designer as it consumes less time during the design stage, and offers flexibility during testing. The moment at which current discharge begins may be selected upon timing calculations or by the aid of displacement sensors [21].

The objective of this study is to introduce a rapid current discharge circuit for muzzle velocity enhancement. The circuit provides an alternative path for rapid current discharge, which eliminates the braking force applied on the projectile, after it crosses the center of the coil. Utilization of the circuit may save precious time in multi-stage coilgun design and testing, as design of the discharge circuit for the last stage guarantees safe operation for the switching-devices in all stages.

The rest of the paper is organized as follows: Section II details the principle of operation of a coilgun system. Section III describes the rapid current discharge circuit, and experimental validation results are given in Section IV. Section V concludes the paper.

II. Coilgun Operation

Coilgun schematic structure is shown in Fig. 2. It is comprised of 4 main components: barrel, solenoid, projectile and drive circuit. The barrel and solenoid are placed around a common axis, and the projectile is propelled through the barrel by the magnetic force generated by an energized coil.

Assuming the capacitor bank is pre-charged, the basic coilgun's operation can be divided into 2 states: charging and freewheeling. Charging state begins when the SCR is turned-ON and the capacitor bank releases its charge to the coil. The equivalent circuit of the charging state is comprised of the capacitor-bank, C, the coil, L, and the loop resistance, R, resulting in an RLC circuit, as shown in Fig. 3a. the coil's

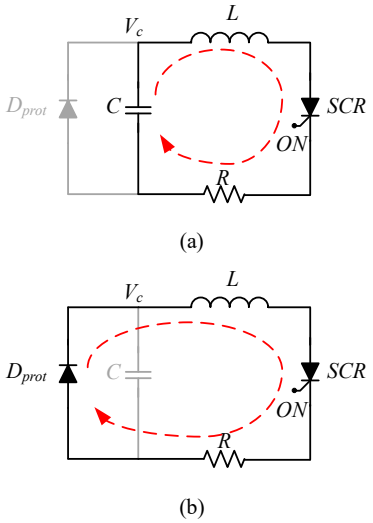

Fig. 3. Equivalent circuits of a single stage coilgun. (a) Charging state. (b) Freewheeling state.

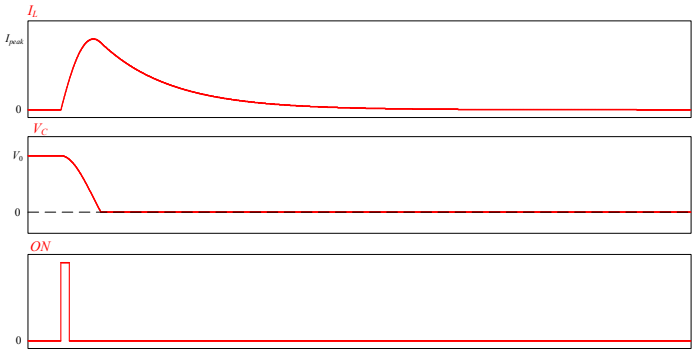

Fig. 4. Typical waveforms of a single stage coilgun.

current can be found by solving the following second-order differential equation:

$$\begin{cases} \frac{d^2}{dt^2} i_L(t) + 2\alpha \frac{d}{dt} i_L(t) + \omega_0^2 i_L(t) = 0 \\ i_L(0) = 0\ A \\ \frac{d}{dt} i_L(0) = \frac{V_0}{L}\ \frac{A}{sec} \end{cases} \quad (1)$$

where i_L is the coil's current, V_0 is the capacitor bank's voltage at the turn-ON instance, ω_0 is the resonance angular frequency and α is the damping factor. Typically, V_0 is in the range of hundreds to thousands of Volts, thus the SCR's forward voltage can be neglected. The high current of the coilgun stages is achieved due to very low loop resistance. Thus, the damping factor, α, is small, and solution of (1) yields:

$$i_L(t) = \frac{V_C(0)}{\omega_d L} sin(\omega_d t)\, e^{-\alpha t}, \quad (2)$$

where $\omega_d = \sqrt{\omega_0^2 - \alpha^2}$.

As can be noted by (2), the current i_L is of a decaying-sinusoidal nature. When the capacitor voltage reverses its polarity the protection diode, D_{prot}, conducts and the freewheeling state begins, as demonstrated in Fig. 4. The equivalent circuit is illustrated in Fig. 3b, and the expression for the coil's current, i_L, during freewheeling state is given by:

$$i_L(t) = \frac{V_C(0)}{\omega_d L} sin(\omega_d t_1)\, e^{-2\alpha(t-t_1)}, \quad (3)$$

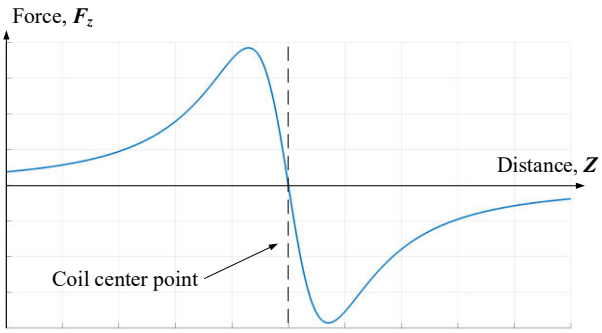

Fig. 5. Force applied on a projectile in the direction of flight.

where $t_1 = \frac{1}{\omega_d} tan^{-1}\left(\frac{-\omega_d}{\alpha}\right)$.

The residual current in the coil produces a braking force, which is applied on the projectile after the projectile's mass center crosses the center of the coil. Fig. 5 illustrates the force applied on a projectile when the current of the coil is constant. Positive force accelerates the projectile in the direction of positive Z-axis. It can be noted that after the projectile crosses the center of the coil it senses braking force, and if this force is constantly applied on the projectile, it will ultimately settle in the center of the coil, which is an equilibrium point. Mitigation of the projectile's braking can be achieved by elimination of the current after the projectile crosses the center point of the coil and is crucial to a high-performance coilgun.

III. Rapid Current Discharge Circuit

A. Circuit Structure

To avoid projectile deceleration the coil current should be discharged as close to zero as possible before the projectile passes through the middle-point of the coil. Due to the high-current at the turn-OFF instance, the current must be rerouted to a branch where the current can be damped quickly. As it is complex to turn-OFF an SCR while current is flowing through it, the discharge circuit elements are added in series with the SCR.

The additional components should offer the ability to discharge the coil as quickly as possible, however, it is not desirable to alter the charging state of the original circuit, and hence, an additional switching-device, that serves as a low impedance path, is added in series with the SCR. Due to the relatively slow switching speeds, and high energy pulses in the circuit an IGBT is selected. The IGBT is turned-ON simultaneously with the SCR and is turned-OFF when the projectile approaches the center of the coil, to commence current discharge.

The value of the coil current is unknown at the turn-OFF instance, and if not rerouted, the current might damage the IGBT due to high voltage spikes produced due to its small parasitic capacitance. Furthermore, it is important to clamp the generated voltage below the IGBT maximum voltage rating. Using a resistor to sustain the coil's current offers a trade-off between the damping time, $\tau=L/R$, and the peak voltage, $V_{peak}=I_L \cdot R$, and is not a viable solution due to large coil inductance and current. A different approach for coil

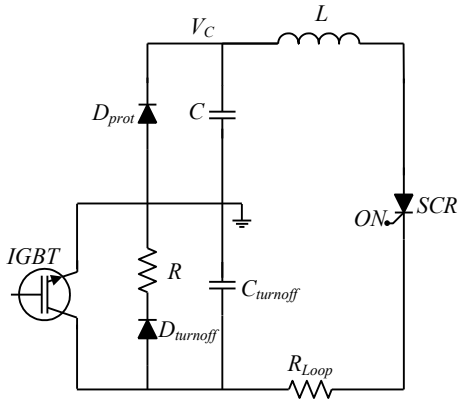

Fig. 6. Schematic circuit of a single stage coilgun with current discharge circuit.

current discharge is by using a voltage source. This method offers flexibility in the selection of the current discharge rate and assists to clamp the IGBT voltage to a safe value when it is turned-OFF. Nevertheless, to avoid short-circuit when the IGBT conducts, it is necessary to decouple the voltage source from it, which adds complexity to the circuit. Moreover, it is impractical to generate a distinct voltage source for each segment in a multi-stage coilgun. A more practical solution is to employ a capacitor parallel with the IGBT.

Fig. 6 illustrates a modified coilgun circuit with a rapid coil current discharge circuit. The main capacitor, C, is pre-charged, and the IGBT and SCR serve as a low impedance path during the charging state. Discharging state commences when the current is redirected towards $C_{turnoff}$, which is done by turning-OFF the IGBT. As the voltage of the capacitor increases, the coil current is reduced until it reaches zero. The duration of the process along with the peak voltage of $C_{turnoff}$ are determined by the values of the passive components. The diode-resistor branch, comprised of R and $D_{turnoff}$, resets the voltage of $C_{turnoff}$ after each pulse.

The turn-OFF instance of the IGBT may occur during the charging state, where the main capacitor, C, still holds charge, or during the freewheeling state, where the diode, D_{prot}, conducts. This leads to two different modes of operation of the current discharge circuit. Typically, it is preferred to switch to discharging state from the freewheeling state, as energy is dissipated during that time, and the current at the switching-instance is relatively low, which reduces the stresses on the discharge circuit. However, in a multi-stage coilgun, the inductance of each coil decreases from stage to stage, while the velocity of the projectile increases. As a result, damping of the coil current must occur earlier with the advancement of each stage. In the first stages, due to the long current pulses, the main capacitor has enough time to discharge to zero, and the circuit enters freewheeling state, before the IGBT is turned-OFF. Nevertheless, as the projectile advances, the IGBT turn-OFF instance precedes from stage to stage, and freewheeling state may not occur. Therefore, both modes of operation are of interest. The equivalent circuits and waveforms of operation in mode I are shown in Fig. 7 and Fig. 8, respectively, as well as the equivalent circuits of operation in mode II, which are illustrated in Fig. 7a and Fig. 9, and their suitable waveforms, which are shown in Fig. 10.

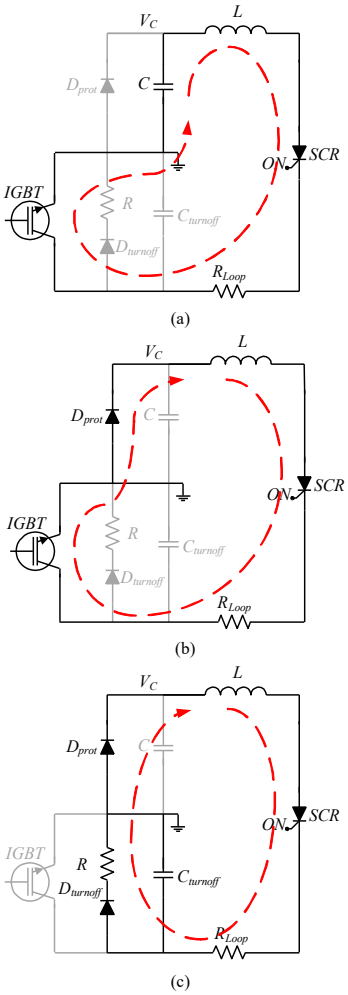

Fig. 7. Equivalent circuits of a single stage coilgun with discharge circuit. Operation mode I. (a) Charging state. (b) Freewheeling state.

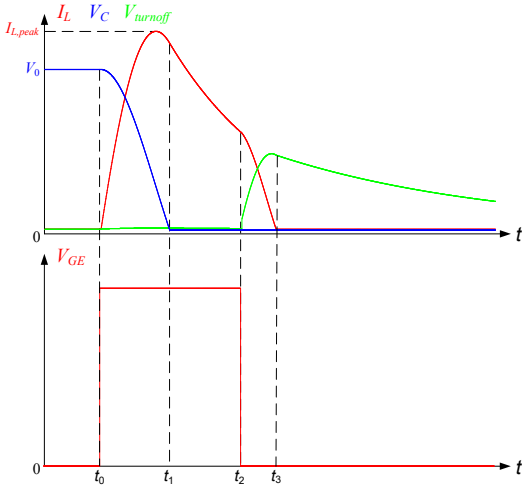

Fig. 8. Typical waveforms of a single-stage coilgun with current discharge circuit. Operation mode I.

B. Operation Mode I

Stage 1 [t_0, t_1]: During this time interval, the SCR and IGBT conduct, and the main capacitor, *C*, charges the coil, *L*. The voltage drops of the SCR and IGBT are negligible compared to the high voltage of *C*, and thus the equivalent circuit is identical to the circuit shown in Fig. 3a. The coil current, i_L, increases and satisfies (2), while the capacitor voltage, V_C, decreases.

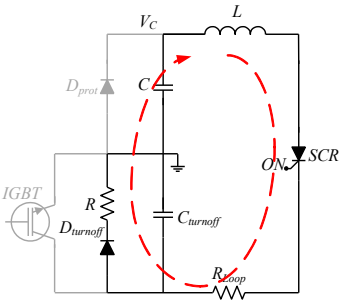

Fig. 9. Equivalent circuit of a single stage coilgun with discharge circuit. Discharging state. Operation mode II.

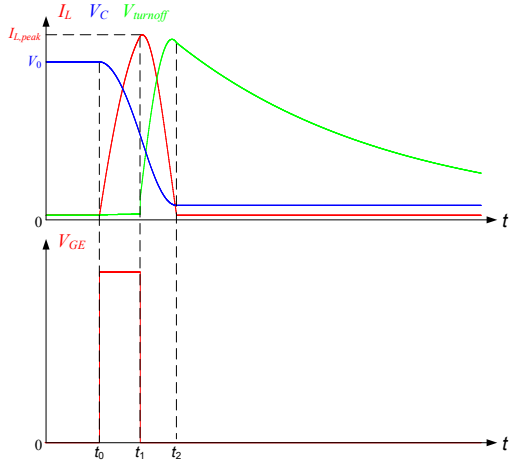

Fig. 10. Typical waveforms of a single-stage coilgun with current discharge circuit. Operation mode II.

Stage 2 [t_1, t_2]: When V_C reverses its polarity, the protection diode, D_{prot}, clamps its voltage to $-V_f$, and the current begins to flow through it. The low forward voltage of the diode has a minor effect on the rate of discharge of the coil current, which is determined by the ratio of the coil inductance and loop resistance.

Stage 3 [t_2, t_3]: The IGBT is turned-OFF, and the current, i_L, is rerouted to the capacitor, $C_{turnoff}$, and diode-resistor branch. The voltage of $C_{turnoff}$ increases, while the coil current rapidly discharges to zero. Commutation of the SCR is obtained when the coil current reaches zero.

This mode of operation is typical to the first several segments of a multi-stage coilgun. The relatively high DCR of the large coils result in high rate of energy dissipation, which lead to low currents at the moment the discharging state commences, and consequently to low stresses on the discharge circuit.

C. Operation Mode II

Stage 1 [t_0, t_1]: This time interval is identical to *Stage 1* of operation mode I.

Stage 2 [t_1, t_2]: When the IGBT is turned-OFF the current is redirected to the capacitor, $C_{turnoff}$, and diode-resistor branch. However, unlike in operation mode I, the current is still flowing through the main capacitor, *C*, and its voltage, V_C, decreases while the coil current and the voltage of $C_{turnoff}$ increase. The peak coil current is obtained when the voltages

of the two capacitors are equal, and at that moment the coil current begins to rapidly discharge. It is obvious from this description that for prompt discharge characteristics, the discharge capacitor's value must be smaller than the main capacitor, namely $C > C_{turnoff}$. V_C may or may not reach zero in this time interval and is dependent on its value at the switching instance, and the discharge time.

This mode of operation is typical for the latter stages of a multi-stage coilgun, where the coils are shorter than in the first segments, and the velocity of the projectile is high. As a result, the duration of the charging state is reduced from segment to segment and the stresses on the discharge circuit are considerably higher than in the first stages. Under these circumstances, design of the discharge circuit for the last segment of a multi-stage coilgun, guarantees that the discharge circuits of all coil segments, can withstand the stresses during the rapid discharge process.

IV. Experimental Validation

To validate the operation of the coilgun with the rapid current discharge circuit, a 450V experimental prototype has been designed, built, and tested. The hardware has been designed on a 2oz., 6-layer PCB, and key components' parameters are listed in Table I.

The capacitor-bank C, is composed of a 1mF/450V electrolytic capacitor, and 50 2.2µF/450V MLCCs, which results in a 1.032mF equivalent capacitor, considering DC bias effect under 420V. IGBT drive voltage is set to 18V.

The shift from charging state to freewheeling is noticeable in the current waveform of Fig. 11. During charging state, the current is of damped-sinusoidal form, and when the main capacitor is fully discharged, the protection diode clamps the capacitor voltage to $-V_f$. During the freewheeling state the energy is dissipated mainly by the loop resistance, and when the projectile approaches the center of the coil, the current is relatively low. Discharging state begins when the IGBT is turned-OFF, 2.5ms after conduction began, and the coil current is diverted into the capacitor $C_{turnoff}$ and the diode-resistor branch. A voltage spike of $V_{turnoff}$ can be seen in Fig, 11, and is due to the capacitor's ESR. The current quickly drops to zero and the capacitor voltage is reset through the diode-resistor branch within a short period of time. The discharge time in this case is approximately 8.5 times quicker than in the case of the system without the discharge circuit, which translates into a muzzle velocity of 15.8 m/s, an improvement of 25.4% compared to 12.6 m/s without the discharge circuit.

As explained in the previous chapters, the first time-interval is identical in both operation modes I and II, and it is visible in Fig. 11 and Fig. 12. In contrast to mode I, in mode II the IGBT is turned-OFF when the main capacitor voltage is non-zero and the coil current is high. The IGBT is turned-OFF after 0.75ms and discharging state begins immediately, skipping the freewheeling stage. The energy diverted into $C_{turnoff}$ is much higher than in operation mode I, as can be seen by the peak voltage of the capacitor – 419V compared to 176V in the previous case.

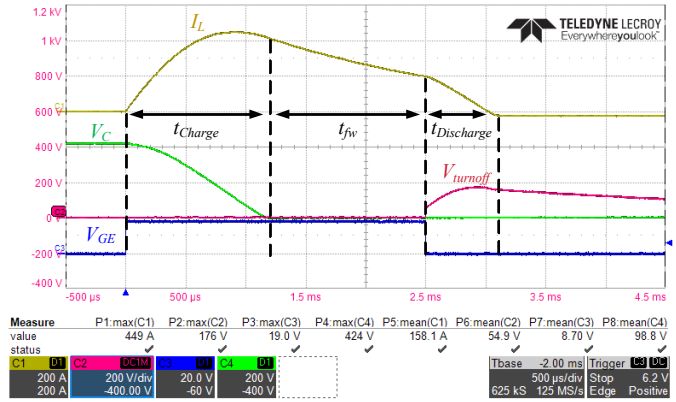

Fig. 11. Experimental waveforms of the prototype with t_{Charge} of 2.5ms. Coil current (yellow) 200A/div, main capacitor voltage (green) 200V/div, discharge capacitor voltage (red) 200V/div, IGBT gate signal (blue) 20V/div, time scale 500µs/div.

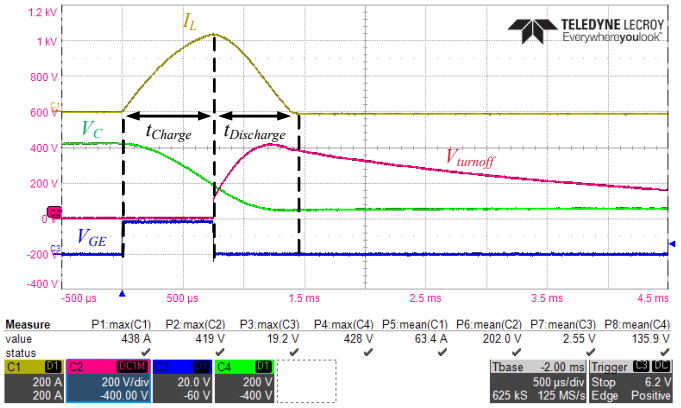

Fig. 12. Experimental waveforms of the prototype with t_{Charge} of 0.75ms. Coil current (yellow) 200A/div, main capacitor voltage (green) 200V/div, discharge capacitor voltage (red) 200V/div, IGBT gate signal (blue) 20V/div, time scale 500µs/div.

TABLE I – Single-Stage Experimental Prototype Components

Component	***Value***
Input voltage V_{in}	420V
Input capacitor C	1.032mF/450V
Coil inductance L	433µH/206mΩ
SCR	600V/50A
Diodes	600V/75A
IGBTs	2 x 600V/370A
Turn-off capacitor $C_{turnoff}$	390µF/450V
Turn-off resistor R	10Ω/20W

V. Conclusion

A rapid current discharge circuit for single and multi-stage coilgun has been presented. The circuit redirects the coil current to an alternative path where it is quickly damped to zero, eliminating the braking force experienced by the projectile after it crosses the center point of the coil. The additional components which comprise the discharge circuit

have a minor effect on the charging and freewheeling states of the coilgun. Two modes of operation are detailed – mode I, which is typical for the first several coil stages, where the coils are large and projectile velocity is low, and mode II, which is prevalent in the latter coil stages, where the velocities are higher. The last stage has the shortest coil, and requires the shortest current pulse, hence the stresses on its discharge circuit are the highest. Design of the discharge circuit to withstand the stresses of the last stage, ensures proper operation for all the previous coil stages, and is extremely advantageous in multi-stage coilgun. The operation modes have been tested and validated on an experimental prototype rated for 450V and built around a 6-layer, 2 oz., PCB, demonstrating rapid coil current discharge and elimination of the braking force on the projectile. Experimental results show an improvement of 25.4% in muzzle velocity of a single-stage coilgun, which is a result of approximately 8.5 times quicker inductor current discharge comparing to the system with no discharge circuit engaged.

ACKNOWLEDGMENT

This research was supported by the ISRAEL SCIENCE FOUNDATION grant number 2186/19.

REFERENCES

[1] Z. Su et al., "Investigation of Armature Capture Effect on Synchronous Induction Coilgun," in *IEEE Transactions on Plasma Science*, vol. 43, no. 5, pp. 1215-1219, May 2015.

[2] R. J. Kaye, "Operational requirements and issues for coilgun electromagnetic launchers," in *IEEE Transactions on Magnetics*, vol. 41, no. 1, pp. 194-199, Jan. 2005.

[3] B. Halivni, M. Evzelman, A. Kuperman and M. M. Peretz, "High Current Pulsed Power Supply for Multi-Stage Induction-Based Acceleration System," *2021 IEEE Applied Power Electronics Conference and Exposition (APEC)*, 2021, pp. 1348-1354.

[4] Y. Hu, Y. Wang, Z. Yan, M. Jiang and L. Liang, "Experiment and Analysis on the New Structure of the Coilgun With Stepped Coil Winding," in *IEEE Transactions on Plasma Science*, vol. 46, no. 6, pp. 2170-2174, June 2018.

[5] B. Go, D. Le, M. Song, M. Park and I. Yu, "Design, Fabrication, and Analysis of a Coil Assembly for a Multistage Induction-Type Coilgun System," in *IEEE Transactions on Plasma Science*, vol. 47, no. 5, pp. 2452-2457, May 2019.

[6] B. Go, D. Le, M. Song, M. Park and I. Yu, "Design and Electromagnetic Analysis of an Induction-Type Coilgun System With a Pulse Power Module," in *IEEE Transactions on Plasma Science*, vol. 47, no. 1, pp. 971-976, Jan. 2019.

[7] M. A. Abdalla and H. M. Mohamed, "Asymmetric Multistage Synchronous Inductive Coilgun for Length Reduction, Higher Muzzle Velocity, and Launching Time Reduction," in *IEEE Transactions on Plasma Science*, vol. 44, no. 5, pp. 785-789, May 2016.

[8] C. Yanjie, L. Wenbiao, L. Ruifeng, Z. Yi and Z. Bengui, "Study of Discharge Position in Multi-Stage Synchronous Inductive Coilgun," in *IEEE Transactions on Magnetics*, vol. 45, no. 1, pp. 518-521, Jan. 2009.

[9] Seog-Whan Kim, Hyun-Kyo Jung and Song-Yop Hahn, "Optimal design of multistage coilgun," in *IEEE Transactions on Magnetics*, vol. 32, no. 2, pp. 505-508, March 1996.

[10] S. Williamson and A. Smith, "Pulsed coilgun limits," in *IEEE Transactions on Magnetics*, vol. 33, no. 1, pp. 201-207, Jan. 1997.

[11] J. A. Andrews, "Coilgun structures," in *IEEE Transactions on Magnetics*, vol. 29, no. 1, pp. 637-642, Jan. 1993.

[12] M. S. Bayati and A. Keshtkar, "Study of the Current Distribution, Magnetic Field, and Inductance Gradient of Rectangular and Circular Railguns," in *IEEE Transactions on Plasma Science*, vol. 41, no. 5, pp. 1376-1381, May 2013.

[13] P. Lehmann, B. Reck, M. D. Vo and J. Behrens, "Acceleration of a Suborbital Payload Using an Electromagnetic Railgun," in *IEEE Transactions on Magnetics*, vol. 43, no. 1, pp. 480-485, Jan. 2007.

[14] S. Hundertmark, G. Vincent, F. Schubert and J. Urban, "The NGL-60 Railgun," in *IEEE Transactions on Plasma Science*, vol. 47, no. 7, pp. 3327-3330, July 2019.

[15] T. Zhang, W. Guo, Z. Su, Y. Liu, W. Fan and H. Zhang, "Optimal Design and Testing of the Driving Coil on Induction Coilgun," in *IEEE Transactions on Plasma Science*, vol. 47, no. 6, pp. 2957-2963, June 2019.

[16] D. Dayan, M. Evzelman and M. M. Peretz, "High-Performance Compact Electromagnetic Coilgun Propulsion System with Low-Voltage Modular Rapid Capacitor Charger," *2020 IEEE Applied Power Electronics Conference and Exposition (APEC)*, 2020, pp. 1559-1566.

[17] A. Hassannia and K. Abedi, "Optimal Switching Scheme for Multistage Reluctance Coilgun," in *IEEE Transactions on Plasma Science*, vol. 49, no. 3, pp. 1241-1246, March 2021.

[18] Z. Su, W. Guo, B. Zhang, M. Li, C. Zhang and J. Li, "The feasibility study of high-velocity multi-stage induction coilgun," *2012 16th International Symposium on Electromagnetic Launch Technology*, 2012, pp. 1-4.

[19] T. Zhang et al., "Acceleration Mechanism and Experimental Research of Multi-Stage Synchronous Induction Coilgun Based on Magnetic Field Arrangement," in *IEEE Transactions on Plasma Science*, vol. 47, no. 10, pp. 4753-4759, Oct. 2019.

[20] M. Song, D. Le, B. Go, M. Park and I. Yu, "Design of an Attractive Force Circuit of Pulsed Power System for Multistage Synchronous Induction Coilgun," in *IEEE Transactions on Plasma Science*, vol. 46, no. 10, pp. 3606-3611, Oct. 2018.